# Disequilibrating azobenzenes by visible-light sensitization under confinement

Julius Gemen[1], Jonathan R. Church[2], Tero-Petri Ruoko[3], Nikita Durandin[3], Michał J. Białek[4], Maren Weißenfels[1], Moran Feller[1], Miri Kazes[1], Magdalena Odaybat[5], Veniamin A. Borin[2], Rishir Kalepu[1], Yael Diskin-Posner[6], Dan Oron[1], Matthew J. Fuchter[5], Arri Priimagi[3], Igor Schapiro[2]*, Rafal Klajn[1,7]*

**Affiliations:**

[1]Department of Molecular Chemistry and Materials Science, Weizmann Institute of Science, Rehovot 76100, Israel.

[2]Fritz Haber Center for Molecular Dynamics Research, Institute of Chemistry, The Hebrew University of Jerusalem, Jerusalem 91904, Israel.

[3]Faculty of Engineering and Natural Sciences, Tampere University, P.O. BOX 541, 33101 Tampere, Finland.

[4]Department of Chemistry, University of Wrocław, 14 F. Joliot-Curie St, 50383 Wrocław, Poland.

[5]Department of Chemistry, Molecular Sciences Research Hub, White City Campus, Imperial College London, 82 Wood Lane, London, UK.

[6]Department of Chemical Research Support, Weizmann Institute of Science, Rehovot 76100, Israel

[7]Institute of Science and Technology Austria, Am Campus 1, 3400 Klosterneuburg, Austria

*Corresponding authors. Emails: rafal.klajn@ista.ac.at; igor.schapiro@mail.huji.ac.il

**Abstract:** Photoisomerization of azobenzenes from their stable *E* isomer to the metastable *Z* state is the basis of numerous applications of these molecules. However, this reaction typically requires ultraviolet light, which limits applicability. Here we introduce DisEquilibration by Sensitization under Confinement (DESC), a supramolecular approach to induce the *E*-to-*Z* isomerization using light of desired color, including red. DESC relies on a combination of a macrocyclic host and a photosensitizer, which act together to selectively bind and sensitize *E*-azobenzenes for isomerization. The *Z* isomer lacks strong affinity for—and is expelled from—the host, which can then convert additional *E*-azobenzenes to the *Z* state. In this way, the host/photosensitizer complex converts photon energy into chemical energy in the form of out-of-equilibrium photostationary states, including ones that cannot be accessed via direct photoexcitation.

**One-Sentence Summary:** A supramolecular complex acts as a catalyst for converting azobenzenes to their metastable state using visible light of desired color.

Azobenzene and its derivatives are arguably the simplest and most widely studied photoswitchable compounds (*1–3*). Upon exposure to UV light, the planar (*4*), nonpolar *E* isomer of azobenzene isomerizes to the metastable *Z* form (Fig. 1A), which is nonplanar and significantly more polar. The *Z*→*E* back-isomerization occurs spontaneously and can be accelerated with blue light. Owing to the highly reversible nature of *E*⇄*Z* photoswitching, azobenzenes and other azoarenes (*5*) have found applications in energy storage systems (*6, 7*), switchable catalysis (*8, 9*), controlled release (*10, 11*), and photopharmacology (*12, 13*), to name but a few (*14, 15*). However, the necessity to rely on UV light to generate the metastable *Z* isomer has severely limited the applicability of these compounds. Shifting *E*-azobenzene's absorption band to the visible range can be achieved by decorating it with various substituents (*16, 17*), but this approach affects the compound's identity and requires additional synthetic effort.

Natural systems evolved an alternative, supramolecular strategy to extend the absorption spectral change of photoswitchable molecules (*18, 19*). For example, deep-sea fishes install a chlorophyll antenna next to the opsin-bound retinal (*20, 21*). This antenna captures red light and sensitizes the nearby retinal via a triplet energy transfer (TET) mechanism (*22*). The subsequent photoisomerization of retinal induces a large conformational change in the surrounding opsin protein, ultimately enabling the fish to detect red light (*23*).

Similar to retinal, azobenzene can be switched via TET (*24–26*). Unfortunately, this process has long (*27, 28*) been known to unidirectionally convert *E*/*Z* mixtures to the thermodynamically stable *E* isomer. This directionality originates from i) the higher tendency of *Z* (over *E*) to act as a triplet energy acceptor (*29*), and ii) the preferential (by a factor of >50 (*28*)) relaxation of the triplet excited state of azobenzene to *E* over *Z*. Therefore, whereas various photosensitizers can rapidly and efficiently facilitate the equilibration of the high-energy *Z* isomer into the stable *E* state, the reverse reaction—i.e., sensitized disequilibration—is far more challenging and has remained elusive.

**The concept of disequilibration by sensitization under confinement (DESC)**

We hypothesized that sensitized disequilibration might be achieved using a photosensitizer (PS) that acts on the *E* isomer of azobenzene with high selectivity (Fig. 1B). We have previously shown that i) the water-soluble, palladium-containing macrocyclic host **H** (*30*) (Fig. 1C) binds two molecules of various *E*-azoarenes (which are planar and readily stack on top of each other to form noncovalent homodimers), but only one molecule in the *Z* configuration (*31, 32*) (because of its nonplanar (*33*) geometry); ii) host **H** can also encapsulate—and thus induce dimerization of—molecules structurally similar to *E*-azobenzene (i.e., planar aromatic molecules), including various dyes (*34, 35*), and iii) mixing two different inclusion complexes (each binding two molecules of a given guest), induces a rapid guest exchange between the hosts, affording heterodimeric complexes, whereby the host encapsulates two different guest molecules (*36*). Taken together, we speculated that host **H** could co-encapsulate the *E* isomer of azobenzene and a PS (thus bringing them in close proximity) while prohibiting close encounters of the same PS with the *Z*-azobenzene (which is bound as a sole guest). We coin this approach DisEquilibration by Sensitization under Confinement (DESC).

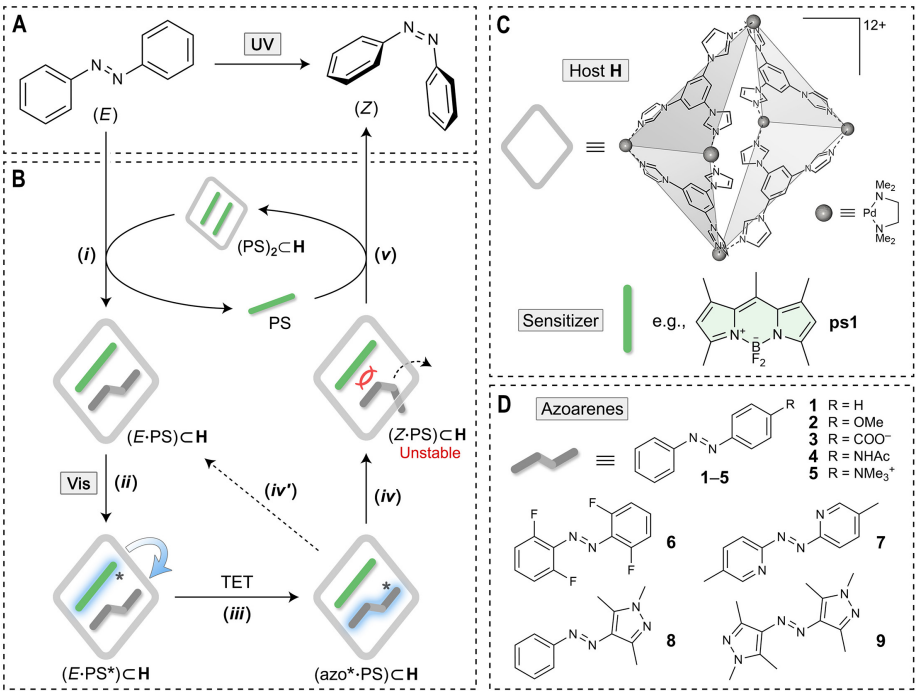


**Fig. 1. Disequilibration by sensitization under confinement (DESC).** (**A**) The transformation of the stable *E* isomer of azobenzene to the metastable *Z* isomer traditionally relies on using ultraviolet ($\lambda \approx 350$ nm) light. (**B**) The mechanism of DESC: (*i*) Formation of the ternary inclusion complex (*E*·PS)⊂**H** (PS = photosensitizer; **H** = host); (*ii*) Absorption of a photon of visible light by the PS followed by ISC; (*iii*) Triplet energy transfer (TET) and the formation of triplet azobenzene, followed by its relaxation (*iv*) to *Z*-azobenzene or, (*iv′*) back to *E*-azobenzene (corresponding to internal conversion); (*v*) Disassembly of the unstable (*Z*·PS)⊂**H** inclusion complex. (**C**) Components of the supramolecular system used for DESC: macrocyclic host **H** coassembled from six $Pd^{2+}$ ions and four triimidazole ligands, and a photosensitizer (here, BODIPY **ps1**). (**D**) Structural formulae of azoarenes **1**–**9** investigated in this study.

The concept of DESC is illustrated in Fig. 1B. The addition of an encapsulated PS (as $(PS)_2$⊂**H**) to *E*-azobenzene induces the formation of a ternary complex (*E*·PS)⊂**H** (step *i*). Upon exposure to visible light, PS is promoted to a singlet excited state, which relaxes to a triplet state via intersystem crossing (ISC) (step *ii*). In step *iii*, PS transfers its triplet energy to the co-confined *E*-azobenzene. The resulting triplet azobenzene—which cannot be generated by direct photoexcitation—can either decay to the initial *E* isomer (step *iv′*) or transform into the *Z* state (step *iv*). The former case regenerates (*E*·PS)⊂**H**, which can be re-excited. In contrast, the latter case results in (*Z*·PS)⊂**H**, which is an unstable complex since *Z*-azobenzene is too bulky to coexist with the PS inside **H**. At the same time, *Z* as a sole guest is bound relatively weakly (fig. S103); hence, it is expelled from the host and effectively removed from the equilibrium. Thus, the azobenzene-free inclusion complex of the PS is regenerated (step *v*) and available for transforming additional molecules of *E*- into *Z*-azobenzene.

To verify our hypothesis, we initially focused on the prototypical azobenzene *E*-**1** and BODIPY dye **ps1** (Fig. 1C, D). Both *E*-**1** and **ps1** form homodimers within **H**'s cavity, as previously elucidated by several techniques, including x-ray diffraction, NMR, and UV/vis absorption spectroscopy (*31, 32, 34*). Figure 2B (dotted brown line) shows the UV/vis spectrum obtained

upon mixing aqueous solutions of the two homodimers—(*E*-**1**)$_2$⊂**H** and (**ps1**)$_2$⊂**H**—in a 1:1 molar ratio. The visible-light absorption profile is practically identical to that of pure (**ps1**)$_2$⊂**H** (blue dotted line), indicating a minute fraction of the (*E*-**1**·**ps1**)⊂**H** heterodimer (i.e., the equilibrium shown in Fig. 2A heavily favors the two homodimers). However, exposing this solution to a low-intensity green light ($\lambda$ = 525 nm, 2.5 mW·cm$^{-2}$) resulted in a substantial (by ~35%) decrease of absorption in the near-UV region (Fig. 2B), indicating the *E*→*Z* isomerization of **1**. This result suggests that the small amount of (*E*-**1**·**ps1**)⊂**H** in equilibrium with the homodimers absorbs green light, the energy of which is eventually used to generate the metastable *Z* isomer (Fig. 1B). The low illumination intensities used in our studies exclude the possibility of two-photon isomerization (*37, 38*), which we confirmed directly by power-dependence experiments (fig. S108).

To determine the scope of DESC, we extended our studies to a diverse portfolio of azobenzenes, including derivatives with electron-donating and -withdrawing substituents, positively and negatively charged groups, and heterocyclic azoarenes (*5*) (**2**–**9** in Fig. 1D). All of these compounds were encapsulated as homodimers within host **H**, as confirmed by NMR spectroscopy (see Supplementary Materials). Similar to **1**, most of these guests preferably existed as *E*$_2$⊂**H** homodimers even in the presence of (**ps1**)$_2$⊂**H**. However, azobispyrazole (*39*) **9** (and, to some extent, azopyrazole (*40*) **8**) showed a strong tendency to form a heterodimer with **ps1**, as manifested by the intense 509 nm peak in the absorption spectrum (Fig. 2C; dotted brown line). The high fraction of the heterodimer allowed us to grow single crystals and solve the structure by x-ray diffraction, revealing *E*-**9** and **ps1** bound tightly inside the cavity of the host (Fig. 2D). Exposure of (*E*-**9**·**ps1**)⊂**H** to 525 nm light quenched its near-UV absorption, consistent with the *E*→*Z* isomerization (Fig. 2C). The putative (*Z*-**9**·**ps1**)⊂**H** heterodimer is unstable, forcing **ps1** into homodimers, which explains why the 400–600 nm portion of the spectrum at the end of the reaction is nearly identical to that of pure (**ps1**)$_2$⊂**H** (Fig. 2C). Similar to **1** and **9**, compounds **2** through **8** also switched to their *Z* isomers when exposed to 525 nm light in the presence of (**ps1**)$_2$⊂**H** (fig. S79).

Interestingly, the vastly different heterodimer populations in **1**+**ps1** vs. **9**+**ps1** mixtures do not translate into major differences in the reaction kinetics: the former comprises only ~2% heterodimer but requires only twice as much time as the latter (with a heterodimer fraction of ~80%) to reach a photostationary state (PSS). This finding reflects the rapid guest exchange kinetics between hosts (*36*), which led us to hypothesize that the DESC should work efficiently also with catalytic amounts of the PS. Indeed, as shown in Fig. 2E, decreasing the amount of (**ps1**)$_2$⊂**H** to only 0.05 equiv. with respect to (*E*-**9**)$_2$⊂**H** extended the time required to reach the PSS fourfold but did not markedly affect its composition.

The finding that *E*-**9** and **ps1** form the heterodimer in a near-quantitative yield allowed us to determine the quantum yield (QY) of DESC for this pair. Here, we note that **ps1** within (*E*-**9**·**ps1**)⊂**H** is highly emissive, but its fluorescence in (**ps1**)$_2$⊂**H** is largely quenched (*34*) – therefore, exposing (*E*-**9**·**ps1**)⊂**H** to a 515 nm pulsed laser led to a gradual decrease of emission (Fig. 2F). When the experiment was repeated in the presence of an extra 2 and 4 equiv. of (*E*-**9**)$_2$⊂**H**, however, we observed lag periods of ~8 and ~18 min, respectively. The stable fluorescence—despite the ongoing *E*→*Z* isomerization of **9**—indicates that the concentration (*E*-**9**·**ps1**)⊂**H** remains steady, which confirms the rapid exchange kinetics in our system: as soon as the isomerized *Z*-**9** is expelled from the host, it is replaced by another copy of *E*-**9** (if available). By assessing the mean number of absorbed photons required to convert the excess of *E*-**9**, we found that each successful *E*→*Z* isomerization event requires 17 photons on average (see Supplementary

Materials for derivation), which corresponds to a QY of ~6% – a remarkably high value, provided the number of steps separating the excitation of **ps1** from the formation of *Z*-**9** (Fig. 1B).

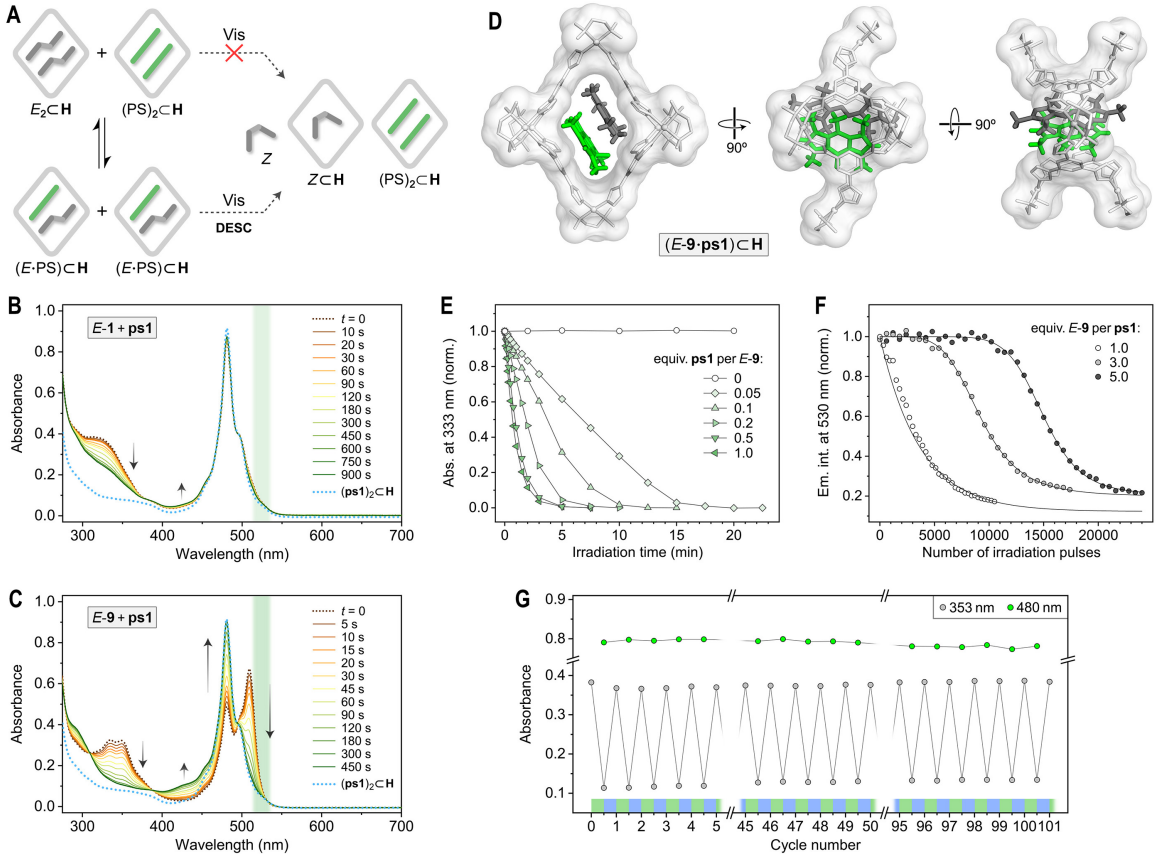


**Fig. 2. Following DESC by steady-state absorption and emission spectroscopy.** (**A**) Equilibrium between (*top*) homodimeric inclusion complexes of a PS and an *E*-azoarene—$(PS)_2\subset\mathbf{H}$ and $E_2\subset\mathbf{H}$, respectively—and (*bottom*) the heterodimeric complex $(E\cdot PS)\subset\mathbf{H}$. Only *E* residing within the heterodimer—but not the homodimer—can be switched with visible light. The resulting *Z* is encapsulated as a sole guest (if enough host is available) and cannot be sensitized either. (**B**) Absorption spectrum of a 1:1 mixture of $(\mathbf{ps1})_2\subset\mathbf{H}$ and $(E\text{-}\mathbf{1})_2\subset\mathbf{H}$ (dotted brown line) and changes in the spectra accompanying irradiation with green light ($\lambda \approx 525$ nm, denoted with green shading). Dotted blue line: absorption spectrum of $(\mathbf{ps1})_2\subset\mathbf{H}$. (**C**) Absorption spectrum of a 1:1 mixture of $(\mathbf{ps1})_2\subset\mathbf{H}$ and $(E\text{-}\mathbf{9})_2\subset\mathbf{H}$ (dotted brown line; predominantly $(E\text{-}\mathbf{9}\cdot\mathbf{ps1})\subset\mathbf{H}$) and changes in the spectra accompanying irradiation with green light. Dotted blue line: absorption spectrum of $(\mathbf{ps1})_2\subset\mathbf{H}$. (**D**) The x-ray crystal structure of the heterodimeric complex $(E\text{-}\mathbf{9}\cdot\mathbf{ps1})\subset\mathbf{H}$ (from the left: front view, side view, and top view; light-gray = host **H**; dark-gray = *E*-**9**; green = **ps1**; water molecules, counterions, and host protons omitted for clarity). (**E**) Following DESC of **9** in the presence of different equivalents of **ps1** (the data were normalized to the 0–1 range, except the experiment with no PS; for raw spectra, see fig. S76). (**F**) Evolution of the emission intensity of **ps1** under 515 nm light (used both to induce DESC and excite fluorescence) as a function of the amount of **9**. (**G**) More than 100 cycles of reversible photoisomerization of **9** induced solely by visible light (*E*→*Z*: DESC with 525 nm light for 2 min; *Z*→*E*: direct photoexcitation using 435 nm light for 30 s). The amount of the *E* isomer is proportional to absorbance at 353 nm; the absorption at 480 nm originates from the $(\mathbf{ps1})_2\subset\mathbf{H}$ homodimer.

Once generated via DESC, the *Z* isomer can be back-isomerized to *E* via direct excitation with blue light (435 nm), and the process can be repeated for many cycles. To demonstrate the robustness of DESC, we subjected compound **9** to >100 switching cycles and did not observe any noticeable fatigue: both **9** and **ps1** retained their initial absorbance values (Fig. 2G).

**Time-resolved spectroscopic and computational studies of DESC**

In solution, BODIPY dyes as simple as **ps1** are poor triplet sensitizers (*41, 42*); therefore, the finding that **ps1** acts as an efficient photosensitizer in DESC is surprising. To obtain mechanistic insights into DESC, we performed transient absorption spectroscopy (TAS) and computational studies (Fig. 3). First, we studied the photoinduced dynamics of the (**ps1**)$_2$⊂**H** homodimer using femtosecond (fs) TAS. Figure 3A shows the fs absorption changes at two different wavelengths, following excitation of (**ps1**)$_2$⊂**H** with a 500 nm laser. The initial (<1 ps) ground-state bleach at 483 nm accompanied by excited-state absorption at 412 nm is indicative of the $S_0 \rightarrow S_1$ transition in **ps1**. At delay times >100 ps, the 412 nm absorption increases further, and the 483 nm bleach becomes more pronounced, which can be attributed to ISC from the $S_1$ to the $T_1$ state (*43*). Using microsecond (μs) TAS, we found the resulting triplet state to be remarkably stable, with a monoexponential lifetime of 16.5±0.5 μs under ambient conditions (fig. S114A). As expected from a triplet state, the lifetime is strongly dependent on the amount of oxygen in the solvent; decreasing the amount of $O_2$ by bubbling $N_2$ for 4 min and 10 min extended the lifetime of the $T_1$ state of **ps1** to 160±4 μs and 10.1±0.5 ms, respectively (fig. S114B).

When the fs-TAS experiment was repeated for a 1:2 mixture of (**ps1**)$_2$⊂**H** and (*E*-**9**)$_2$⊂**H** (i.e., a pair with a high tendency to form a heterodimer), the bleach at 483 nm was significantly less pronounced (Fig. 3B, inset), indicating a TET to *E*-**9** (see step *iii* in Fig. 1B). Importantly, the TET and the subsequent formation of *Z*-**9** occur in the ns time regime, i.e., much faster than the lifetime of the **ps1** triplet state, which explains why DESC does not require exclusion of oxygen. In fact, we found the process to be equally efficient in strictly deoxygenated vs. thoroughly oxygenated water (fig. S91).

We also studied the *E*-**9**/**ps1** pair under ambient conditions by μs-TAS (Fig. 3C) and found the intensity of transient absorption at 430 nm within 0.1 μs after excitation ($\Delta Abs^{*}_{430}$) to be inversely proportional to the amount of (*E*-**9**)$_2$⊂**H**, consistent with the quenching of the **ps1**'s triplet state by its *E*-**9** co-guest via TET. The resulting triplet-**9** can either relax to the initial *E*-**9** isomer or switch to *Z*-**9**, which absorbs at 430 nm – hence the increasing steady-state absorption ($\Delta Abs^{\infty}_{430}$). This intimate relationship between the degree of **ps1** triplet state quenching and the extent of *E*→*Z* isomerization identified by μs-TAS further confirms that DESC proceeds via TET between the **ps1** donor and *E*-**9** acceptor.

To gain further insights into DESC, we studied various azoarene/PS combinations as noncovalent heterodimers using quantum chemical simulations. We consistently found that the lowest-energy triplet state within these heterodimers was localized on the PS (therefore, we refer to it as $T_{PS}$) and the second-lowest triplet state was localized on the azoarene (i.e., $T_{azo}$), indicating that the $T_{PS} \rightarrow T_{azo}$ transition is an endothermic process (*25, 44*) (e.g., see Fig. 3D for the energy diagram of **1**·**ps1**). These results led us to hypothesize that the experimentally observed TET might be facilitated by thermal fluctuations of molecules, as suggested previously for other triplet donor–acceptor pairs (*25, 26, 45, 46*). Therefore, we studied the variation of the **1**·**ps1** excited state energies on the C–N=N–C dihedral angle ($\Phi$) in azobenzene **1** (which is significantly more flexible than **ps1**). Figure 3E shows a relaxed scan for the **1**·**ps1** heterodimer, demonstrating that an 18º

twist in $\Phi$ is sufficient to invert the energetic order of $T_{\mathbf{ps1}}$ and $T_{E\text{-}\mathbf{1}}$, making TET energetically favorable. We separately studied the dynamics of the (**1**·**ps1**)⊂**H** heterodimer by multiscale MD simulations (Movie S1); these simulations reveal that thermal fluctuations readily allow **1** to adopt conformations with $\Delta\Phi \geq 18°$ at room temperature.

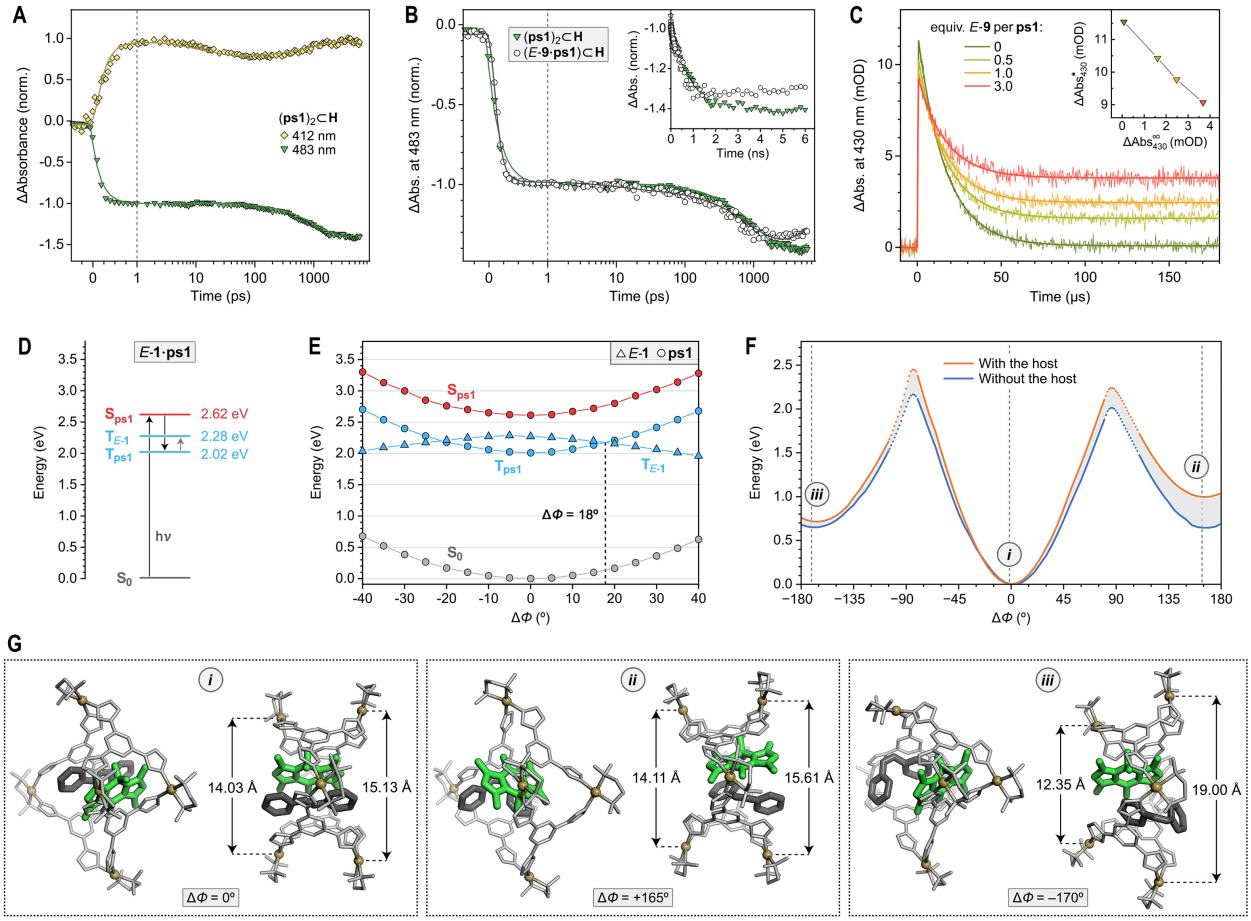


**Fig. 3. Time-resolved spectroscopic and computational studies of DESC.** (**A**) Normalized decays of fs transient absorption of **ps1** at 412 nm and 483 nm within the (**ps1**)$_2$⊂**H** homodimer ($\lambda_{exc}$ = 500 nm). Points: raw data; lines: four-exponential fits (see Supplementary Materials for details). (**B**) Normalized transient absorption decays of **ps1** at 483 nm ($\lambda_{exc}$ = 500 nm) in (**ps1**)$_2$⊂**H** vs. the (*E*-**9**·**ps1**)⊂**H** heterodimer (linear scale in the 0–1 ps time range; logarithmic scale beyond 1 ps). Inset: the same data plotted on the linear scale. (**C**) Decays of μs transient absorption at 430 nm ($\lambda_{exc}$ = 510 nm) in (**ps1**)$_2$⊂**H** in the presence of increasing amounts of (*E*-**9**)$_2$⊂**H**. The thin and thick lines correspond to experimental data and biexponential fits, respectively. Inset: the inverse correlation between $\Delta Abs^{*}_{430}$ (absorbance at 430 nm immediately after photoexcitation) and $\Delta Abs^{\infty}_{430}$ (steady-state absorbance). All the TAS results presented here were collected under ambient (non-deoxygenated) conditions. (**D**) The calculated energies of the $S_1$, $T_{\mathbf{ps1}}$, and $T_{E\text{-}\mathbf{1}}$ states in the *E*-**1**·**ps1** heterodimer (see Fig. S116 for details). The arrows indicate the sequence of events (the symbol "h$\nu$" indicates a photoinduced transition; the light arrow indicates an endothermic process). (**E**) Ground-state relaxed scan along the C–N=N–C dihedral angle $\Phi$ in **1** within the **1**·**ps1** heterodimer. The black, red, and blue lines denote the ground state, the bright singlet state, and the two lowest triplet states, respectively. The green and gray markers correspond to the

localization of the excited state on the donor (**ps1**) and acceptor (**1**), respectively. (**F**) Ground-state relaxed scan of $\Phi$ in **1** within the (**1**·**ps1**)⊂**H** heterodimer (orange trace). The blue trace shows the energies corresponding to the same configurations of **1** and **ps1** after removing the host and its interactions. The scan was performed with the QM/QM2 hybrid scheme. (**G**) Optimized geometries of (**1**·**ps1**)⊂**H** for the three $\Delta\Phi$ values indicated in panel F (*left:* side views; *right:* top views). The distances between the indicated equatorial Pd nodes describe the degree of host deformation; the larger the difference between the two Pd–Pd distances, the greater the transition of **C** from a tube-like conformation into a bowl-like conformation.

We also performed QM/QM2 simulations to better understand the relative instability of the (*Z*·PS)⊂**H** heterodimers vs. (*E*·PS)⊂**H** (see Fig. 1B), which lies at the heart of efficient DESC. The starting point of the simulations was (*E*-**1**·**ps1**)⊂**H** with a perfectly planar geometry of *E*-**1** ($\Phi$ = 180º). We performed a relaxed scan by changing $\Phi$ in steps of 5º in both senses of rotation; the resulting energies are plotted in Fig. 3F in orange. The blue curves in Fig. 3F correspond to the same geometries while neglecting the host and its interactions; therefore, the energetic difference between the two curves (highlighted as gray shading) quantifies the instability of the inclusion complex. We found that rotating $\Phi$ in one direction affords a highly unstable supramolecular architecture *ii* (Fig. 3G, *center*) that is ~0.35 eV (~8 kcal/mol) higher in energy than free *Z*-**1**·**ps1** (Fig. 3F). Interestingly, rotating $\Phi$ in the opposite direction gave rise to a geometry where the host did not markedly increase the energy (*iii* in Fig. 3F and G). However, in this structure, host **H** assumes a bowl-like conformation, and *Z*-**1** extrudes from the cavity, facilitating its expulsion to the solution (Movies S3–S6). The high conformational flexibility of **H** (*47*) is an important requirement for DESC; in fact, the cavities of rigid coordination cages (*48*) and other confined environments (*49, 50*) were shown to render azobenzene non-photoswitchable.

**Tuning the excitation wavelength of DESC**

Encouraged by the unexpected sensitization potency of **ps1** under confinement, we considered DESC with other, more red-shifted dyes, including ones not previously known to act as triplet sensitizers. To this end, we first focused on the fluorinated BODIPY **ps2** (Fig. 4A), with an absorption peak centered at ~553 nm (*51*) (compared with 499 nm for **ps1**). We found that **ps2** exhibited a higher affinity than **ps1** to form heterodimers with various azoarenes; the increased PS–azoarene interactions should further promote DESC. Indeed, Fig. 4B shows that **ps2** induces a near-quantitative *E*→*Z* conversion of an equimolar amount of azobenzene **4** within only 90 s of low-intensity (2.5 mW·cm$^{-2}$) yellow light (561 nm) irradiation. Moreover, the more efficient DESC allowed us to decrease the PS loading further: at only 0.01 equiv. of (**ps2**)$_2$⊂**H** with respect to (*E*-**4**)$_2$⊂**H**, the PSS was reached within ~20 min (Fig. 4C).

In general, **ps2** is a more efficient DESC agent than **ps1**. However, we found one exception: **ps2** proved unable to induce the switching of azobispyrazole *E*-**9**. To understand this result, we resorted to quantum chemical simulations and found the $T_{PS}$–$T_{azo}$ energy gap for the *E*-**9**·**ps2** heterodimer to be exceptionally high (1.03 eV; compared to 0.26 eV for *E*-**1**·**ps1** in Fig. 3D). Moreover, relaxed scans analogous to those in Fig. 3E show that $\Phi$ in **9** must twist by 38º—a prohibitively large distortion—for the energies of these two triplet states to cross (fig. S122D). These computational results not only rationalize the experimental findings but provide further (although indirect) support for the involvement of the TET mechanism in our system.

We also worked with resorufin **ps3** and resazurin **ps4** (Fig. 4A), both previously reported to form inclusion complexes of the (PS)$_2$⊂**H** type (*35*). These two dyes are red-shifted even further; for

example, the absorption maxima of the respective heterodimers with *E*-**1** appear at 587 nm and 616 nm, with absorption extending into the red spectral range. To our satisfaction, exciting the absorption bands on these heterodimers with orange and red light, respectively, resulted in a highly efficient *E*→*Z* isomerization of nearly all azoarene/PS combinations (Figs. 4D, F).

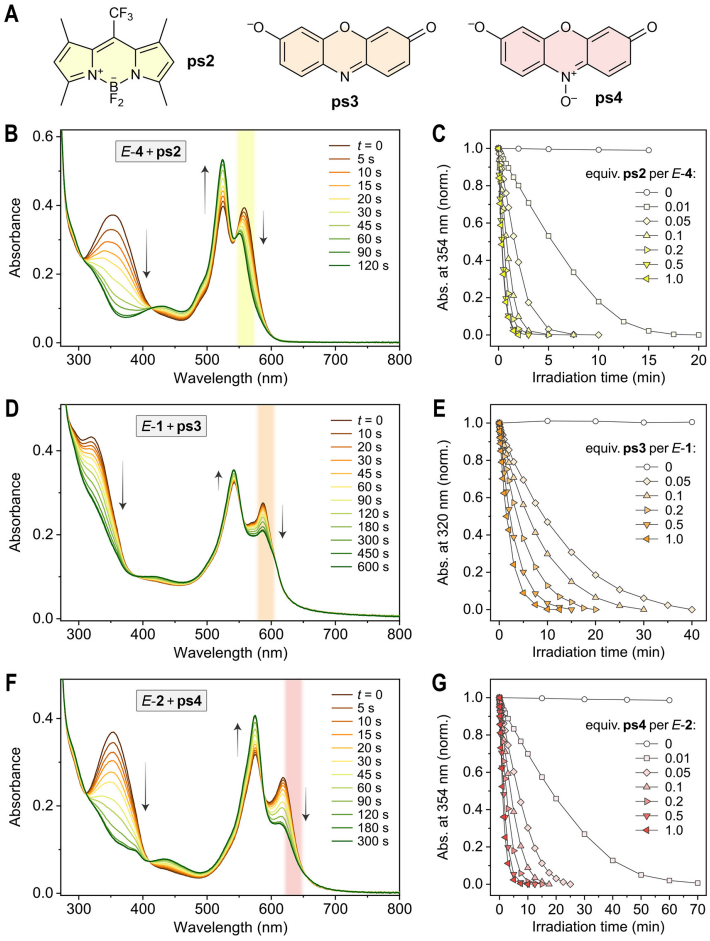


**Fig. 4. Extending the concept of DESC to red-shifted photosensitizers.** (**A**) Structural formulae of fluorinated BODIPY **ps2**, resorufin **ps3**, and resazurin **ps4**. (**B**) Changes in the absorption spectra of encapsulated *E*-**4** in the presence of an equimolar amount of encapsulated sensitizer **ps2** under yellow light ($\lambda \approx 561$ nm, 2.5 mW·cm$^{-2}$). (**C**) DESC (here, for *E*-**4**) in the presence of substoichiometric amounts of **ps2**. (**D**) Changes in the absorption spectra of encapsulated *E*-**1** in the presence of an equimolar quantity of encapsulated sensitizer **ps3** under orange light ($\lambda \approx 599$ nm, 0.8 mW·cm$^{-2}$). (**E**) DESC (here, for *E*-**1**) in the presence of substoichiometric amounts of **ps3**. (**F**) Changes in the absorption spectra of encapsulated *E*-**2** in the presence of an equimolar quantity of encapsulated sensitizer **ps4** under red light ($\lambda \approx 635$ nm at 3.4 mW·cm$^{-2}$). (**G**) DESC (here, for *E*-**2**) in the presence of substoichiometric amounts of **ps4**. The data in C, E, and G were normalized to the 0–1 range, except for the experiments with no PS; for raw data, see figs. S85G, S93F, and S98G, respectively.

The performance of DESC is showcased in Fig. 5A, which lists the PSS compositions (blue font) for all the nine model azoarenes shown in Fig. 1D (encapsulated within **H** in water with 0.05 equiv.

of the selected sensitizer; **ps2** for **1**–**7** and **ps1** for **8** and **9**). The reactions were performed on the NMR scale (i.e., milligram quantities of **1**–**9**) and can readily be scaled up to obtain the *Z* isomers on the preparative scale (tens of milligrams). As control experiments (red font), we irradiated **1**–**9** under the same conditions and in the presence of the PS but without host **H** (hence, in an organic solvent). In the absence of **H**, the *E* isomers could not be co-confined with the PS, which resulted in negligible amounts of *Z* isomer formation via direct photoexcitation (only azobenzene **6**, known for its visible-light-responsiveness (*17*), afforded a sizeable (14%) amount of *Z*). We note that the positively charged azobenzene (*52*) **5** (often recognized as a prototypical photopharmacophore (*13, 53*)) showed a particularly impressive contrast in behavior between the presence and absence of the host, giving rise to 98% of *Z*. Notably, such a *Z*-rich PSS cannot be achieved by direct photoisomerization (of neither (*E*-**5**)$_2$⊂**H** or free **5**) with any wavelength of light (the same is true for compounds **1**, **3**, and **6**) because of the partial overlap of the absorption bands of the two isomers (*54*). In contrast, the PSS composition in DESC is dictated by the tendency of the two isomers to form the ternary (azo·PS)⊂**H** complex, and this tendency is overwhelmingly higher for the *E* isomer.

Having demonstrated that the positively charged *E*-**5** can be successfully transformed into *Z*-**5** despite its low affinity to the like-charged **H**, we speculated that other water-soluble azobenzenes may also be efficiently disequilibrated using a substoichiometric amount of not only the PS but also the host. Figure 5B shows the result of an experiment in which an aqueous solution of the negatively charged **3** was exposed to red light in the presence of 0.005 equiv. of (**ps4**)$_2$⊂**H**. The absorption spectrum of this solution is dominated by the intense absorption peak of *E*-**3** in the near-UV region; the small amount of the sensitizer appears as a weak band at ~600 nm (Fig. 5B). Remarkably, exciting this band with low-intensity 635 nm light resulted in a near-complete disappearance of the much more prominent peak originating from another species (*E*-**3**). We found that the PSS contained 88% of *Z*-**3** (vs. ~0% in the absence of either **H** or **ps4**), indicating that each molecule of **H** hosted more than 180 *E*→*Z* isomerization events on average.

**Photoswitching selectivity enabled by DESC**

To further demonstrate the potential of DESC, we explored the cavity size and charge (+12) of host **H** to discriminate between photoreactive compounds with overlapping absorption bands, and which otherwise cannot be converted selectively. To this end, we mixed *E*-**3** and *E*-**5** in a 1:3 ratio and added (**ps2**)$_2$⊂**H** (0.5 equiv. with respect to **3**; Fig. 5C). At low (micromolar) concentrations, only the negatively charged **3** exhibits a strong affinity to **H**; **5** is not encapsulated owing to the Coulombic repulsion. Indeed, yellow light (561 nm) illumination of this mixture led to a highly selective switching of *E*-**3** (despite the threefold excess of *E*-**5** (Fig. 5D and fig. S104). In contrast, exposure to UV light induced nonselective switching of both azobenzenes via direct excitation. In the second example, we worked with a mixture of *E*-**4** and 9-bromoanthracene, both in the form of encapsulated homodimers with **H**. Upon exposure to UV light, the encapsulated anthracene rapidly dimerizes to afford the corresponding dianthracene (*36*) under the same irradiation conditions that trigger the direct *E*→*Z* photoisomerization of **4** (Fig. 5E, right). However, exposing the same mixture to yellow light in the presence of (**ps2**)$_2$⊂**H** induced highly selective photoisomerization of azobenzene, leaving the anthracene intact (Fig. 5F, dotted line).

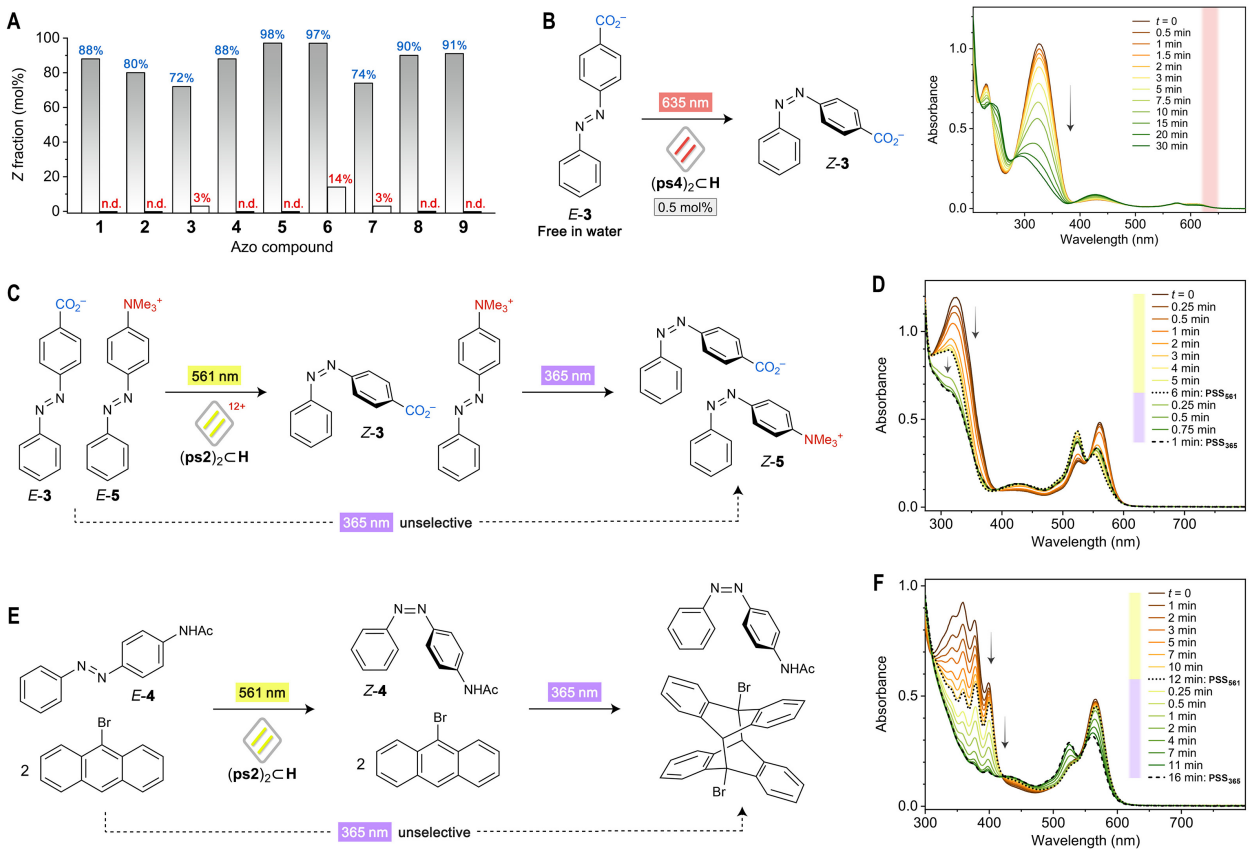


**Fig. 5. Performance and selectivity of DESC.** (**A**) *Blue font:* Composition of the photostationary state (PSS) of azoarenes **1**–**9** subjected to DESC on the millimolar scale in the presence of 0.05 equiv. of the PS (**ps2** under 561 nm light for **1**–**7**; **ps1** under 525 nm light for **8** and **9**). *Red font:* PSS compositions of the same azoarene/PS mixtures under the same illumination conditions but in the absence of the host ($CDCl_3$ was used as the solvent, except **3** and **5**, where $CD_3OD$ used). Illumination times: 15, 12, 35, 12, 40, 24, 45, 4, and 9 min for **1**–**9**, respectively. "n.d." = "not detected" (i.e., the amount of *Z* below the NMR detection limit). (**B**) Red-light switching of *E*-**3** dissolved in water in the presence of 0.005 equiv. of **(ps4)$_2$⊂H** affords a PSS featuring 88% *Z*-**3**. (**C**) Selective switching of the negatively charged *E*-**3** with 561 nm light in the presence of the positively charged *E*-**5** on the micromolar scale. (**D**) The corresponding absorption spectra. Dotted line: PSS under 561 nm light; dashed line: PSS after the subsequent exposure to 365 nm light (both azobenzenes isomerize to a similar extent). (**E**) Selective switching of *E*-**4** with 561 nm light and **(ps2)$_2$⊂H** in the presence of a UV-dimerizable anthracene. (**F**) The corresponding UV/vis absorption spectra. Dotted line: PSS under 561 nm light; dashed line: after the subsequent exposure to 365 nm light.

## Discussion

From the thermodynamics perspective, our system acts as a light-driven supramolecular machine that converts light into chemical energy in the form of out-of-equilibrium photostationary states. DESC relies on the selective co-encapsulation of the stable (*E*) isomer of an azobenzene with a dye that acts as an antenna, capturing visible light whose energy is ultimately used to generate the metastable *Z* isomer. The absorption of light promotes the dye from the ground state to the singlet excited state. Confinement inside the host increases the dye's ability to undergo intersystem crossing populating the dye's triplet state and turning it into a potential triplet sensitizer. Quantum chemical simulations reveal that although the triplet state of azobenzene is higher than that of the dye, a small dihedral angle twist in azobenzene lowers its triplet energy while increasing the triplet energy of the co-encapsulated dye to the extent that the two energy levels converge. Therefore, the dye-to-azobenzene triplet energy transfer can become favorable owing to azobenzene dynamics (*25, 44*). Once in the triplet state, the azobenzene can either dissipate energy or switch to the *Z* isomer. Z-azobenzene is nonplanar and can no longer be co-confined with the photosensitizer; thus, it is expelled from the host and cannot be re-sensitized. In this way, DESC shifts the equilibrium towards the metastable *Z* state without the need to populate azobenzene's singlet excited state, which is relatively high in energy and requires the absorption of UV light.

Although we focused on a particular host and one class of photoswitchable molecules (**H** and azoarenes, respectively), our results allow us to establish general design principles for new DESC systems:

1. The host should have an affinity to a photoswitch and a photosensitizer, and its cavity should be large enough to simultaneously encapsulate the photosensitizer and the thermodynamically stable isomer of the photoswitch.

2. The host's affinity to the metastable form of the photoswitch is significantly lower (because of its different shape and/or polarity) – therefore, it can no longer be co-encapsulated with the photosensitizer.

3. Open cavity and/or conformational flexibility: the host should have rapid guest binding and release kinetics for fast catalytic turnover and to ensure that once generated, the metastable form of the photoswitch is expelled from the cavity before it is re-sensitized.

In principle, DESC is applicable to other classes of photoswitchable compounds, although larger or differently shaped hosts may be required. Self-assembly via metal–ligand coordination offers an attractive approach to generating a wide range of hosts from simple components in a modular fashion.

As demonstrated in this work, DESC is a robust process that works with catalytic amounts of sensitizers, under ambient conditions (no oxygen exclusion necessary), and for a wide range of aromatic and heterocyclic azoarenes. We envision that DESC will become a powerful tool to control chemical reactivity through a combination of light irradiation and confinement.

**References and Notes**


1. G. S. Hartley, *Nature* **140**, 281 (1937).
2. H. M. D. Bandara, S. C. Burdette, *Chem. Soc. Rev.* **41**, 1809–1825 (2012).
3. F. A. Jerca, V. V. Jerca, R. Hoogenboom, *Nat. Rev. Chem.* **6**, 51–69 (2022).
4. T. Tsuji, H. Takashima, H. Takeuchi, T. Egawa, S. Konaka, *J. Phys. Chem. A* **105**, 9347–9353 (2001).
5. S. Crespi, N. A. Simeth, B. König, *Nat. Rev. Chem.* **3**, 133–146 (2019).
6. Z. Wang *et al.*, *Joule* **5**, 3116–3136 (2021).
7. M. Le, G. G. D. Han, *Acc. Mater. Res.* **3**, 634–643 (2022).
8. R. S. Stoll, S. Hecht, *Angew. Chem. Int. Ed.* **49**, 5054–5075 (2010).
9. Y. Wei, S. Han, J. Kim, S. Soh, B. A. Grzybowski, *J. Am. Chem. Soc.* **132**, 11018–11020 (2010).
10. J. Lu, E. Choi, F. Tamanoi, J. I. Zink, *Small* **4**, 421–426 (2008).
11. D. Tarn *et al.*, *Nanoscale* **6**, 3335–3343 (2014).
12. W. A. Velema, W. Szymanski, B. L. Feringa, *J. Am. Chem. Soc.* **136**, 2178–2191 (2014).
13. K. Hüll, J. Morstein, D. Trauner, *Chem. Rev.* **118**, 10710–10747 (2018).
14. J. M. Mativetsky *et al.*, *J. Am. Chem. Soc.* **130**, 9192–9193 (2008).
15. R. Klajn, P. J. Wesson, K. J. M. Bishop, B. A. Grzybowski, *Angew. Chem. Int. Ed.* **48**, 7035–7039 (2009).
16. A. A. Beharry, O. Sadovski, G. A. Woolley, *J. Am. Chem. Soc.* **133**, 19684–19687 (2011).
17. D. Bléger, J. Schwarz, A. M. Brouwer, S. Hecht, *J. Am. Chem. Soc.* **134**, 20597–20600 (2012).
18. S. P. Balashov *et al.*, *Science* **309**, 2061–2064 (2005).
19. A. Chazan *et al.*, *Nature* **615**, 535–540 (2023).
20. J. K. Bowmaker, *Vision Res.* **48**, 2022–2041 (2008).
21. T. Isayama *et al.*, *Nature* **443**, 649–649 (2006).
22. A. Valentini, M. Nucci, L. M. Frutos, M. Marazzi, *ChemPhotoChem* **3**, 925–932 (2019).
23. R. H. Douglas *et al.*, *Nature* **393**, 423–424 (1998).
24. J. Moreno, M. Gerecke, L. Grubert, S. A. Kovalenko, S. Hecht, *Angew. Chem. Int. Ed.* **55**, 1544–1547 (2016).
25. J. Isokuortti *et al.*, *Chem. Sci.* **12**, 7504–7509 (2021).
26. P. Bharmoria *et al.*, *Chem. Sci.* **13**, 11904–11911 (2022).
27. L. B. Jones, G. S. Hammond, *J. Am. Chem. Soc.* **87**, 4219–4220 (1965).
28. E. Fischer, *J. Am. Chem. Soc.* **90**, 796–797 (1968).

29. F. Strieth-Kalthoff, M. J. James, M. Teders, L. Pitzer, F. Glorius, *Chem. Soc. Rev.* **47**, 7190–7202 (2018).
30. D. Samanta, S. Mukherjee, Y. P. Patil, P. S. Mukherjee, *Chem. Eur. J.* **18**, 12322–12329 (2012).
31. D. Samanta *et al.*, *Proc. Natl. Acad. Sci. U.S.A.* **115**, 9379–9384 (2018).
32. A. I. Hanopolskyi *et al.*, *Beilstein J. Org. Chem.* **15**, 2398–2407 (2019).
33. A. Mostad, C. Rømming, *Acta Chem. Scand.* **25**, 3561–3568 (1971).
34. J. Gemen, J. Ahrens, L. J. W. Shimon, R. Klajn, *J. Am. Chem. Soc.* **142**, 17721–17729 (2020).
35. O. Yanshyna, M. J. Białek, O. V. Chashchikhin, R. Klajn, *Comm. Chem.* **5**, 44 (2022).
36. J. Gemen *et al.*, *Chem* **8**, 2362–2379 (2022).
37. H. Ishitobi, Z. Sekkat, S. Kawata, *J. Chem. Phys.* **125**, 164718 (2006).
38. C.-K. Lim *et al.*, *Nanoscale* **8**, 4194–4202 (2016).
39. A. Gonzalez *et al.*, *J. Am. Chem. Soc.* **144**, 19430–19436 (2022).
40. C. E. Weston, R. D. Richardson, P. R. Haycock, A. J. P. White, M. J. Fuchter, *J. Am. Chem. Soc.* **136**, 11878–11881 (2014).
41. M. A. Filatov, *Org. Biomol. Chem.* **18**, 10–27 (2020).
42. I. Kähärä *et al.*, *Photochem. Photobiol. Sci.* **21**, 1677–1687 (2022).
43. R. P. Sabatini *et al.*, *J. Phys. Chem. Lett.* **2**, 223–227 (2011).
44. K. Sandros, H. L. J. Bäckström, *Acta Chem. Scand.* **16**, 958–968 (1962).
45. J. Eng, T. J. Penfold, *Chem. Rec.* **20**, 831–856 (2020).
46. S. A. Mavrommati, S. S. Skourtis, *J. Phys. Chem. Lett.* **13**, 9679–9687 (2022).
47. L. Pesce, C. Perego, A. B. Grommet, R. Klajn, G. M. Pavan, *J. Am. Chem. Soc.* **142**, 9792–9802 (2020).
48. T. Kusukawa, M. Fujita, *J. Am. Chem. Soc.* **121**, 1397–1398 (1999).
49. A. B. Grommet, L. M. Lee, R. Klajn, *Acc. Chem. Res.* **53**, 2600–2610 (2020).
50. R. Wang *et al.*, *J. Electroanal. Chem.* **438**, 213–219 (1997).
51. S. Choi, J. Bouffard, Y. Kim, *Chem. Sci.* **5**, 751–755 (2014).
52. J. Bieth, S. M. Vratsanos, N. Wasserman, B. F. Erlanger, *Proc. Natl. Acad. Sci. U.S.A.* **64**, 1103–1106 (1969).
53. M. M. Lerch, M. J. Hansen, G. M. van Dam, W. Szymanski, B. L. Feringa, *Angew. Chem. Int. Ed.* **55**, 10978–10999 (2016).
54. E. Fischer, *J. Phys. Chem.* **71**, 3704–3706 (1967).
55. J. Gemen *et al.*, Disequilibrating azobenzenes by visible-light sensitization under confinement, Dryad (2023); https://dx.doi.org/10.5061/dryad.4qrfj6qg1.

**Acknowledgments:**

**Funding:** We acknowledge funding from the European Union's Horizon 2020 Research and Innovation Program (European Research Council (ERC) grants 820008 (RK) and 101045223 (AP) and Marie Skłodowska-Curie grants 812868 (JG) and 101022777 (TPR)), the Academy of Finland (Center of Excellence Programme LIBER, grant 346107 (AP), Flagship Programme PREIN, grant 32016 (AP), and Postdoctoral Researcher grant 340103 (TPR)), Zuckerman STEM Leadership Program Fellowship (JRC), President's PhD Scholarship (MO), and the EPSRC (Established Career Fellowship, grant EP/R00188X/1) (MJF).

**Author contributions:**

Conceptualization: AP, IS*, RK*; methodology: JG, JRC, TPR, ND, DO, AP, IS*, RK*; investigation: JG, TPR, ND, MJB, MW, MF, MK, MO, VAB, RK, YDP; funding acquisition: MJF, AP, IS*, RK*; project administration: RK*; supervision: DO, MJF, AP, IS*, RK*; writing: JG, JRC, TPR, ND, AP, IS*, RK*.

**Competing interests:** The authors declare no competing interests.

**Data and materials availability:** Crystallographic data for inclusion complexes (*E*-**9**)$_2$⊂**H**, (*E*-**9**·**ps1**)⊂**H**, and (**TX**)$_2$⊂**H** have been deposited in the Cambridge Crystallographic Data Centre (CCDC) with accession codes 2240153, 2227254, and 2227255. All other data are available in the main text or the supplementary materials. Raw data underlying the plots have been deposited at https://dx.doi.org/10.5061/dryad.4qrfj6qg1.

**Supplementary Materials**

Materials and Methods

Supplementary Text

Figs. S1 to S122

Tables S1 to S5

Movies S1 to S6

References (*56*–*94*)